DOI: 10.13009/EUCASS2017-288

Parabolized stability analysis of chemically reacting boundary layer flows in equilibrium conditions

L. Zanus, F. Miró Miró and F. Pinna†
Aeronautics and Aerospace Department, von Karman Institute for Fluid Dynamics
Chaussée de Waterloo 72, 1640 Rhode-Saint-Genèse, Belgium
ludovico.zanus@vki.ac.be · fernando.miro.miro@vki.ac.be · fabio.pinna@vki.ac.be
†Corresponding author

6th July 2017

Abstract

Stability of self-similar hypersonic flows over a flat plate in presence of local thermodynamic equilibrium conditions is studied by means of linear Parabolized Stability Equations (PSE). A spectral collocation numerical method together with a finite difference-based marching scheme are used to solve the equations, while the gas mixture and transport properties are computed with a table look-up procedure. High temperature effects are found to destabilize the second Mack mode regardless of the adiabatic/isothermal wall condition considered. On the other hand, nonlocal effects show a Mach-dependence influence: stabilizing at lower Mach, while destabilizing at higher ones.

1. Introduction

Laminar-turbulent boundary layer transition is a key aspect in the design phase of vehicles traveling at hypersonic speeds, such as future cruise spaceplanes and atmospheric re-entry capsules. When a flow undergoes the turbulent regime, severe increments in drag and heat flux are observed on the body surfaces, compromising not only the vehicle performances but also its integrity. Accurate physics-based engineering tools to estimate transition locations are thus of paramount importance in order to reduce the design margins and build more efficient and cheaper vehicles. A practical example is the optimization of re-entry spacecraft Thermal Protection Systems (TPS), where a proper sizing of the heat shield can avoid the employment of additional material, reducing the overall system weight and mission costs.

Despite the continuous advancement of our knowledge about the fluid stability and transition phenomenon, many questions still have to be answered. This is particularly true in regard to hypersonic flows (see for an overview Reed et al.[22,23]), due to the difficulties in conducting ground test and in-flight experiments and the complexity in modeling high temperature gas flows. For these reasons, in order to have accurate stability analysis and reliable transition predictions in high Mach regimes, both advanced transition and aerothermodynamic models are required.

Calculations based on Linear Stability Theory (LST) represent the most widespread technique to conduct boundary layer stability analysis. In this framework the flow is considered inhomogeneous only along the direction normal to the wall (i.e. parallel flow assumption), thus neglecting nonlocal effects such as the boundary layer growth and curvature. On the other hand, the Parabolized Stability Equations (PSE) method[10,9] overcomes this drawback by extending the stability investigation to flows weakly dependent also on the streamwise direction. Moreover, with the nonlinear PSE development[1,2] the transition process can be described up to the turbulent onset, which makes the PSE results comparable in accuracy to the DNS ones, but at a much lower computational cost.

Stability studies at high Mach regimes dealing with high temperature effects such as chemical reactions and vibrational energy relaxation, have extensively preferred the LST framework over other stability techniques. Malik et al.[16] assumed the flow to be in thermal and chemical equilibrium (i.e. Local Thermodynamic Equilibrium, LTE), Stuckert et al.[27] introduced in the analysis finite rate chemistry (i.e. Chemical NonEQuilibirum, CNEQ), while Hudson et al.[11] considered the effect of both thermal and chemical nonequilibrium (i.e. TCNEQ). All these studies proved that high temperature effects bring a non-negligible contribution to the boundary layer stability. In fact, in presence of reactions and vibrational relaxation the thermal boundary layer usually cools down, leaving the flow more subjected to second-mode disturbances. The first extension of the PSE technique to high enthalpy flows is due to Chang et al.[4] for LTE conditions, and Johnson et al.[13] for TCNEQ. Despite the fact that some PSE codes have been developed in

DOI: 10.13009/EUCASS2017-288

the past, there is no extensive literature about their application to hypersonic flows. Moreover, the problems reported often concern validations against in-flight or ground test experiments (see for example Malik[15] and Johnson et al.[12]), while there is a lack of benchmark results which could help a direct verification of a new PSE code. The PSE analysis of high Mach flows highlighted a modification of the disturbances growth rate peaks levels and positions, compared to their LST counterparts, leading to direct and sensible consequences not only on stability, but also on transition-location estimations. Moreover, specific features like detection of unstable supersonic modes, not visible in the parallel flow limit assumption, were found[4], even if not yet fully explained.

In this work the stability of hypersonic flows over adiabatic and isothermal flat plates, in chemical and thermal equilibrium, is studied by means of linear PSE. The influence on the nonparallel effects of infinite rate chemistry and transport and thermodynamic properties variations is investigated at different Mach numbers. The PSE solver employed was developed in the framework of the VKI Extensible Stability and Transition Analysis (VESTA) toolkit[20]. The PSE algorithm, originally written only for flows in Calorically Perfect Gas (CPG) conditions, has been extended to include flows in LTE regime. The results described in this work represent a first verification of the new code and a step towards the inclusion of finite rate chemistry and nonlinearities.

2. Problem formulation

2.1 Governing equations

The Navier-Stokes equations for a gas mixture in local thermodynamic equilibrium do not formally change compared to the ones describing a calorically perfect gas. The fact that chemical reactions occur, in this case at an infinite rate, leads to variable specific heats, and makes internal energy and transport properties depend on any two thermodynamic variables (here chosen as pressure and temperature) instead of the sole temperature dependence for CPG flows. Being the continuity and momentum equations purely mechanical in nature, they are not influenced by the chemistry, while the energy equation slightly modifies compared to the one in CPG conditions, since the effect of diffusion has to be included and enthalpy can not longer be written as a simple multiplication of temperature and specific heat at constant pressure. The Navier-Stokes equations are given in nondimensional invariant form for a gas in LTE conditions, in absence of body forces. Superscripts q^i denote vectorial contravariant variables, whereas subscripts q_i denote vectorial covariant variables (see Pinna et al.[21]). Also, indexes following a comma denote spatial derivatives (e.g. $u^i_{,j} = \partial u^i / \partial x^j$).

$$\frac{\partial \rho}{\partial t} + (u^j \rho)_{,j} = 0 \tag{1a}$$

$$\rho \frac{\partial u^i}{\partial t} + \rho u^j u^i_{,j} = -g^{ij} p_{,j} + \frac{1}{Re} \mathbb{T}^{ij}_{,j} \tag{1b}$$

$$\rho \frac{\partial h}{\partial t} + \rho u^j h_{,j} = Ec \left(\frac{\partial p}{\partial t} + u^j p_{,j} \right) + \frac{1}{RePr} q_f{}^j_{,j} + \frac{Ec}{Re} g_{ik} \mathbb{T}^{kj} u^i_{,j} \tag{1c}$$

where g^{ij} is the metric tensor, ρ the density, u^i the velocity component in different spatial directions, p the pressure, h the enthalpy and $\mathbb{T}$ the stress tensor defined as:

$$\mathbb{T}^{ij} = \lambda g^{ij} u^k_{,k} + \mu \left(g^{jk} u^i_{,k} + g^{ik} u^j_{,k} \right) \tag{2}$$

where μ and λ are respectively the first and second viscosity coefficients. Moreover, the heat flux, neglecting radiation and the Dufour's effect, takes the form

$$q_f{}^j = -k_{fr} g^{ij} T_{,j} + \sum_{s=1}^{n_s} h_s J_s^j = k_{eq} g^{ij} T_{,j} \tag{3}$$

where T is the temperature, k_{fr} the "frozen" thermal conductivity, J_s^j the diffusion mass flux of the s^{th} species and k_{eq} is an equivalent thermal conductivity, here used to rewrite the equation in terms of a Fourier's law. The nondimensionalization, whose details are described in §2.2.2, leads to the appearance of the Reynolds number Re, Prandtl number Pr and the Eckert number Ec.

For a gas in LTE conditions the mixture molecular weight variation has to be taken into account, thus the equation of state, with the apex $\hat{}$ denoting dimensional quantities, becomes:

$$\hat{p} = \hat{\rho} \frac{\hat{\mathscr{R}}}{\hat{\mathscr{M}}_{diss}} \hat{T}, \quad \text{where} \quad \hat{\mathscr{M}}_{diss} = \left(\sum_{s=1}^{n_s} \frac{\hat{C}_s}{\hat{\mathscr{M}}_s} \right)^{-1} \tag{4}$$

DOI: 10.13009/EUCASS2017-288

in which $\hat{\mathscr{M}}_{diss}$ is the molecular weight of the dissociated gas mixture, $\hat{C}_s$ and $\hat{\mathscr{M}}_s$ are respectively the mass fraction and molecular weight of the s^{th} species and $\hat{\mathscr{R}}$ is the universal gas constant. Eq. (4) can be simplified by introducing the compressibility factor $\zeta = \hat{\mathscr{M}}_{undiss}/\hat{\mathscr{M}}_{diss}$ and the specific gas constant of the undissociated gas R_e

$$\hat{p} = \hat{\rho} R_e \hat{T} \zeta \tag{5}$$

which in nondimensional form reads:

$$Hp = \rho T \zeta \tag{6}$$

where $H = Ec \cdot c_{pe}/R_e$. Eq. (1) together with Eq. (6) constitute the problem governing system of equations, which has to be closed by the definition of the transport and thermodynamic gas mixture properties through proper modeling.

2.1.1 Mixture gas properties

In the LTE limit, flow properties depend on the variable mixture composition, which is defined by the minimization of its Gibbs free energy with proper mass balance constraints (see Scoggins et al.[26]). An air-5 model (N_2, O_2, N, O, NO) with undissociated composition of 79% N and 21% O is adopted in this work, which takes into account the following reactions:

$$\begin{gathered} N_2 \rightleftarrows 2N \\ O_2 \rightleftarrows 2O \\ NO \rightleftarrows N + O \end{gathered} \tag{7}$$

Transport and thermodynamic properties are obtained from the library MUTATION++ based on kinetic theory (see Magin et al.[14] and Scoggins et al.[25]). Tables of gas properties are generated within the library in the pressure range $200 - 8000\ Pa$ and temperature range $50 - 5000\ K$. The desired values are then obtained by interpolation from these tables.

For the computations within the calorically perfect gas model, transport properties are assumed being dependent only from the temperature, trough the Sutherland's law. The first viscosity coefficient $\hat{\mu}$ is thus modeled according to:

$$\hat{\mu} = \hat{\mu}_{ref} \left(\frac{\hat{T}}{\hat{T}_{ref}} \right)^{\frac{3}{2}} \cdot \frac{\hat{T}_{ref} + \hat{S}}{\hat{T} + \hat{S}} \tag{8}$$

where, if not otherwise specified

$$\begin{gathered} \hat{\mu}_{ref} = 1.716 \cdot 10^{-5}\ Kg/(m \cdot s) \\ \hat{T}_{ref} = 273.15\ K \\ \hat{S} = 110.6\ K \end{gathered} \tag{9}$$

For the second viscosity coefficient Stokes's hypothesis is applied, thus $\hat{\lambda} = -\frac{2}{3}\hat{\mu}$. Thermal conductivity is also automatically defined since constant Prandtl number and specific heat (respectively equal to $Pr = 0.7$ and $c_{pe} = 1.0045\ kJ/(kgK)$, if not otherwise specified) are assumed, hence $\hat{k} = c_{pe}\hat{\mu}/Pr$. An air gas constant $R_e = 287.05\ J/(kgK)$ is adopted.

2.2 Parabolized Stability Equations

Parabolized Stability Equations are derived by following the classic approach adopted in perturbation theory. Every flow quantity q is decomposed into a mean part $\bar{q}$, the laminar base flow, plus a perturbation component q':

$$q(x^i, t) = \bar{q}(x^i) + q'(x^i, t) \tag{10}$$

Contrary to LST, the parallel flow assumption is not applied within the PSE framework, meaning that the base flow depends not only on wall-normal direction, but also on the streamwise one. The latter dependence though is considered "weak", in the sense that the flow variation over one disturbance wavelength is negligible. The spanwise component however, is not taken into account in this work, since only 2D flows are studied.

By inserting the expression (10) into the Navier-Stokes equations, subtracting the equation satisfied by the base flow and dropping second and higher order terms (linearization), the equations governing the motion of the perturbations are obtained. The main concept of the PSE development rests on the decomposition of every disturbance (or mode) q' into a slowly varying amplitude (or shape) function and a fast-oscillatory wave function:

$$q'(x^1, x^2, x^3, t) = \underbrace{\tilde{q}(x^1, x^2)}_{\text{shape function}} \underbrace{\exp\left(\int_{x_0^1}^{x^1} \alpha(\xi) d\xi + \beta x^3 - \omega t \right)}_{\text{wave function}} + c.c. \tag{11}$$

DOI: 10.13009/EUCASS2017-288

where *c.c* denotes the complex conjugate. This decomposition is appropriate as long as the perturbations and their characteristics vary slowly in the streamwise direction (allowing the simplification $\tilde{q}_{,11} = 0$) and they are subjected eventually only to convective instability. Substituting the ansatz (11) into the perturbation equations and applying the aforementioned hypothesis the PSE in CPG and LTE conditions are obtained. Regardless of the aerothermodynamic model used, the equations can be rearranged in the matrix form:

$$\underline{\underline{L}}\,\underline{\tilde{q}} + \underline{\underline{M}}\,\underline{\tilde{q}}_{,1} + \alpha_{,1}\underline{\underline{Na}}\,\underline{\tilde{q}} = 0 \tag{12}$$

where $\underline{\tilde{q}} = [\tilde{u}^1, \tilde{u}^2, \tilde{u}^3, \tilde{T}, \tilde{p}]$ is the vector of the perturbation variables and the $\underline{\underline{L}}$, $\underline{\underline{M}}$ and $\underline{\underline{Na}}$ matrices are functions of the mean flow quantities and the stability parameters.

In order to solve the problem, Eq. (12) is not sufficient, since the variation of α introduces one additional unknown. The way to close the problem is solving the ambiguity in the decomposition (10). This is translated in imposing a proper normalization condition on $\underline{\tilde{q}}$ at a fixed boundary height location or in an averaged sense, by means of an integral norm. Following the explanation in[9], the desired closure expression finally takes the form:

$$\int_\Omega \underline{\tilde{q}}^\dagger \underline{\tilde{q}}_{,1}\, dy = 0 \tag{13}$$

where Ω indicates the domain in x^2. Different normalization conditions can be employed depending on the selected $\tilde{q}$ components. Chang et al.[3] showed that the PSE results are basically independent on the chosen norm and on the x^2 location it is applied. Different norms lead to different partitions (11), but the physical solution $\underline{q'}$ substantially does not change. In this work we chose to normalize by considering all the five elements of the $\underline{\tilde{q}}$ vector.

2.2.1 Initial and boundary conditions

Eq. (12) and Eq. (13) constitute an initial boundary value problem. Hence a proper initialization and boundary conditions are required. Homogeneous boundary conditions are applied for the temperature and velocity components both at the wall and at the boundary layer edge. A compatibility condition is instead applied on the pressure variable: in this case it consists in rewriting the x^2-momentum equation at the boundaries. In summary we have:

$$\begin{aligned} \tilde{u}^i = \tilde{T} = 0, \quad \tilde{p}_{,2} = X_0 \qquad \text{at } x^2 = 0 \\ \tilde{u}^i = \tilde{T} = 0, \quad \tilde{p}_{,2} = X_e \qquad \text{at } x^2 = x_e^2 \end{aligned} \tag{14}$$

where X_0 and X_e represent the remaining terms of the x^2-momentum equation. Initial conditions are obtained by performing a local LST calculation, thus in general:

$$\underline{\tilde{q}} = \underline{\tilde{q}}_{LST} \quad \text{at } x^1 = {x^1}_0 \tag{15}$$

2.2.2 Nondimensionalization and scaling considerations

All variables are nondimensionalized according to their free stream values, denoted by the subscript e. The reference quantities are length δ_e, velocity U_e, time δ_e/U_e, density ρ_e, temperature T_e, pressure p_e, enthalpy h_e, viscosity μ_e λ_e, and conductivity k_e. The free stream dynamic pressure has been chosen for the nondimensionalization: $p_e = \rho_e {U_e}^2$.

Fixed quantities are used as reference in the PSE computation: U_{e0}, ν_{e0} (kinematic viscosity) and δ_{e0}, which give the fixed Reynolds number $Re_0 = U_{e0}\delta_{e0}/\nu_{e0}$. The reference length scale is defined according to the Blasius scale

$$\delta_e(\hat{x}^1) = \sqrt{\frac{\nu_{e0}\,\hat{x}^1}{U_{e0}}} \tag{16}$$

In this way $\delta_{e0} = \delta_e(\hat{x}^1_0)$, where $\hat{x}^1_0$ is an arbitrary reference position. In the current implementation all the quantities have been nondimensionalized according to the correspondent reference values at the initial marching position. In particular, this leads to the equivalence $Re_0 = x^1_0 = \hat{x}^1_0/\delta_{e0}$. The nondimensional frequency is defined as $F = 2\pi\hat{f}\nu_{e0}/{U_{e0}}^2$, where $\hat{f}$ is in Hertz, which satisfies the relation $F = \omega/Re_0$.

On the contrary, local stability analysis uses the local length scale $\delta_e(\hat{x}^1)$ (also referred in the following as l_e) and Reynolds number $Re = U_e\delta_e/\nu_e$. All the results presented in this work are converted, in the postprocessing of the PSE solution, to the local scale (denoted here with the superscript *, but dropped in the following). For this purpose it is useful to recall the following relations:

$$\alpha^* = \alpha\frac{Re}{Re_0} \quad \omega^* = \omega\frac{Re}{Re_0} \quad Re = \sqrt{xRe_0} \tag{17}$$

DOI: 10.13009/EUCASS2017-288

2.2.3 Measures of growth

Within the PSE theory, perturbations grow and decay with different rates. In general the growth rate of a quantity $\tilde{q}$ can be written as:

$$\gamma_{\tilde{q}} = -\Im(\alpha) + \Re\left(\frac{1}{\tilde{q}}\tilde{q}_{,1}\right) \tag{18}$$

According to the quantity $\tilde{q}$, different definitions are possible. The ones used in this work are based on:

- maximum of the streamwise fluctuation ${u^1}''_{max} : \tilde{q} = \tilde{u}^1$
- maximum of the mass flux fluctuation $(\rho u^1)''_{max} : \tilde{q} = (\rho u^1)'$, where

$$(\rho u^1)' = (\tilde{\rho}\bar{u}^1 + \bar{\rho}\tilde{u}^1) \tag{19}$$

where the symbol $''$ denotes what in the experiments is the root-mean-square of the physical perturbation profile, mathematically equal to the module of the relative perturbation q'. In addition, in the same way, it is possible to define the physical wave number as:

$$\sigma = \Re(\alpha) + \Im\left(\frac{1}{\tilde{q}}\tilde{q}_{,1}\right) \tag{20}$$

2.3 Numerical implementation

The tools used in this work to perform the stability computations have been developed within the VESTA toolkit[20]. The derivation of the PSE equations in both CPG and LTE conditions was done by means of the VESTA Automatic Derivation and Implementation Toolkit (AD&IT) written in Maxima and Matlab languages (see Groot[8] and Pinna[21]). It consists of a computer algebra system, which allows to obtain stability equations for different stability theories, flow regimes and coordinate systems, in an automatic, error-free manner. It has to be highlighted that the two different types of aerothermodynamic models refer to two different PSE analytic developments, meaning that the CPG solutions are not obtained as a limit of the LTE equations. PSE constitutes an initial boundary value problem, solvable by a marching technique. A first order backward Euler method is used to discretize the streamwise derivatives, while the wall-normal ones are approximated by a Chebyshev spectral collocation method based on Lagrangian polynomia defined on Gauss-Chebishev-Lobatto points. A Malik mapping is adopted to cluster points close to wall, to have a better resolution of the boundary layer. The same spectral method and mapping procedure are also used to perform spatial LST calculations: global solutions of the eigenvalue problems are obtained by means of a QZ algorithm, while a local solver based on a Newton eigenvalue-searching technique performs sweepings over different Reynolds numbers. All the mean flows considered were calculated from the self-similar boundary layer solution, both for the CPG and LTE assumption. For further details about the numerical method generally used in VESTA and the structure of the PSE algorithm refer respectively to Pinna[20] and Zanus[28].

3. Results

The verification of the CPG PSE solver was already done in Zanus[28]. The verification of the LTE solver is here done through a comparison against literature results for a wide range of Mach numbers: from subsonic to high supersonic and hypersonic regimes. In facts, nothing prevents to use the PSE LTE code also in the CPG limit, while its correct implementation still can be tested. The verification test cases consist of adiabatic and isothermal flat plate flows, on which 2D disturbances (i.e. $\beta = 0$) are analyzed. The subsonic and supersonic studied cases are reported in Tab. 1, with the corresponding literature references. In the following, the superscript $\hat{}$ denoting dimensional quantities has been dropped.

Table 1: Studied test cases in subsonic and supersonic regimes

M_e	T_e $[K]$	p_e $[Pa]$	F	Ref.
0.5	206	1500	$4.00 \cdot 10^{-5}$	Bertolotti[1]
1.6	206	1500	$4.00 \cdot 10^{-5}$	Bertolotti[1]
4.5	123	1500	$1.53 \cdot 10^{-4}$	Salinas[24]

The first comparison is done against the PSE results of Bertolotti[1] in CPG conditions, for two flows respectively at Mach 0.5 and 1.6. The same computations were performed by means of PSE and LST, both in the CPG and in

DOI: 10.13009/EUCASS2017-288

the LTE limits, in order to highlight respectively eventual nonparallel and high temperature effects. Fig. 1 shows, as expected, that in low Mach regime the calorically perfect gas assumption holds. The growth rate curves of the first Mack mode obtained by the CPG and LTE solvers basically superimpose each other in the $M_e = 0.5$ case and present a minimal shift in the $M_e = 1.6$ one. Nonparallel effects are known to be negligible for 2D modes on a flat plate flow. Nevertheless, as the Mach increases, an accentuated shift of the growth rate curve towards higher Re numbers and a reduction of the maximum peak is visible. This show a slight tendency to stabilize the flow. Both PSE codes reproduce the literature results with good accuracy.

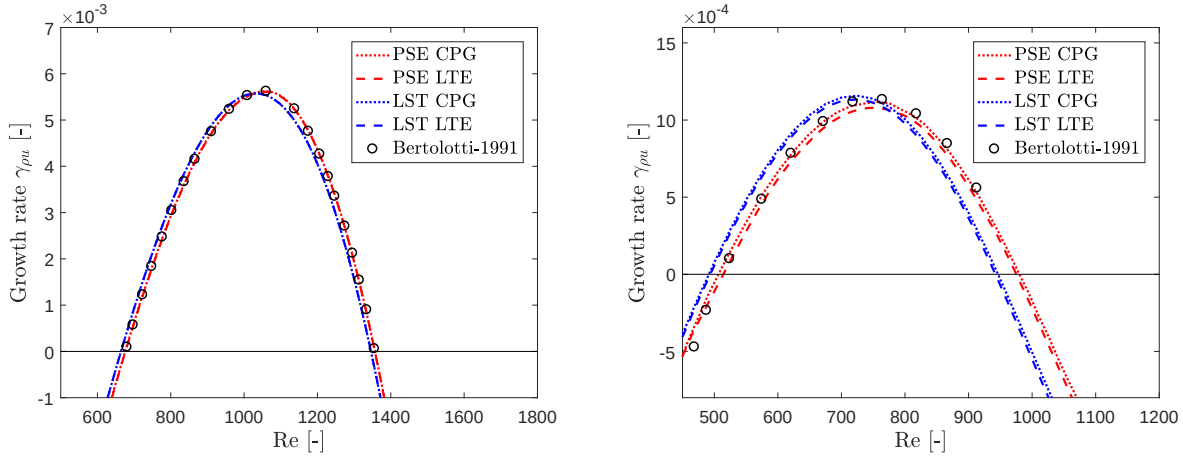

Figure 1: Growth rate in both CPG and LTE conditions: comparison against PSE in Bertolotti[1] and LST results. Flow cases: $M_e = 0.5$, $T_e = 206\,K$, $F = 4.00 \cdot 10^{-5}$ (right), $M_e = 1.6$, $T_e = 206\,K$, $F = 4.00 \cdot 10^{-5}$ (left)

The second verification features a Mach 4.5 flow previously studied by Salinas[24], by means of PSE in CPG conditions. In this case the so-called second Mack mode is excited. Contrary to the previous test cases, the effect of the local thermodynamic assumption is here more visible and produces the same consequences regardless of the stability theory considered. It leads to a shift of the growth rate curve towards higher Re numbers and an increment of the maximum peak, hence it has a destabilizing effect. On the other hand, by comparing PSE and LST results of the same aerothermodynamic model, it is clear that nonparallelism increases the instability region of the mode, moves the peak position towards higher Re, but at the same time lowers it, resulting in a slight stabilization.

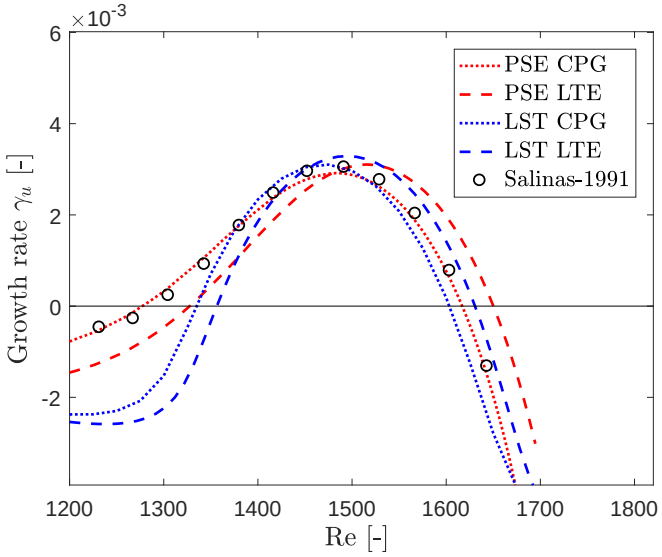

Figure 2: Growth rate in both CPG and LTE conditions: comparison against PSE in Salinas[24] and LST results. Flow case: $M_e = 4.5$, $T_e = 123\,K$, $F = 1.53 \cdot 10^{-4}$

DOI: 10.13009/EUCASS2017-288

The differences between the LTE and CPG results are not due to flow chemistry in this case (the compressibility factor ζ is constantly equal to 1 across the boundary layer), but to the different physical and transport models. Even if the flow is non-reactive, it is possible to have for example variable specific heats due to molecules vibrational excitation. Fig. 3 shows the comparison between the two models for the dynamic viscosity and the thermal conductivity coefficients. There are evident discrepancies between the curves modeled by the empirical Sutherland's law and the ones computed by MUTATION++.

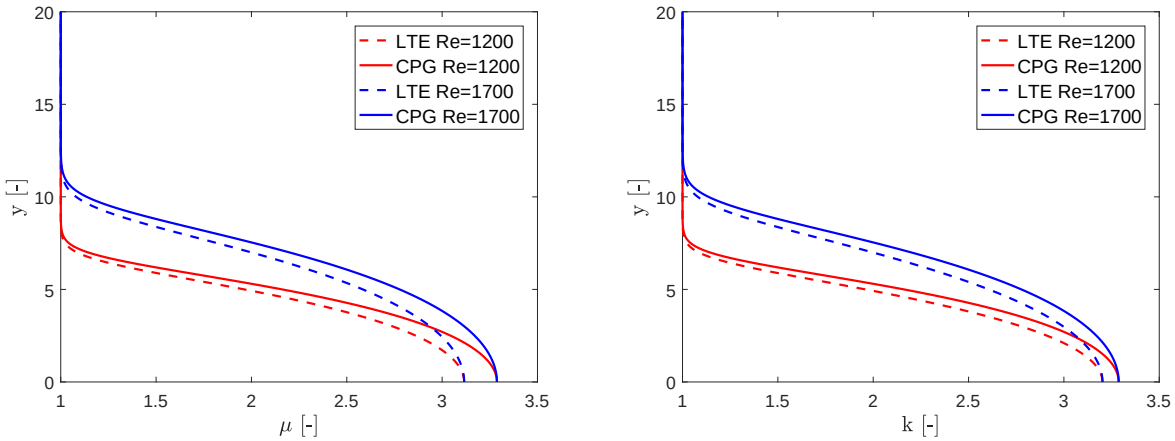

Figure 3: Nondimensional first viscosity and thermal conductivity coefficients in CPG and LTE conditions at different streamwise locations. Flow case: $M_e = 4.5$, $T_e = 123\,K$, $F = 1.53 \cdot 10^{-4}$, $Re_0 = 800$

The chosen cases to directly verify the PSE solver against literature results computed in LTE, are the flat plates studied by Malik et al.[16] by means of LST and reproduced also by Marxen et al.[19] by means of DNS (see Tab. 2). Fig. 4 compares VESTA nondimensional streamwise velocity and temperature self-similar mean flow profiles against the results obtained by Marxen et al.[19], with Navier-Stokes equations, and by Malik et al.[16] by solving the boundary layer equations. In order to compare the results in CPG conditions, the reference quantities in Sutherland's law were changed according to the values reported in[16]. There is overall a good agreement with the DNS solution, but a remarkable difference compared to Malik et al.[16]. This is due to different calculations of the gas mixture properties. Marxen et al.[19], in fact, coupled their CFD solver with the MUTATION library, a previous version of MUTATION++.

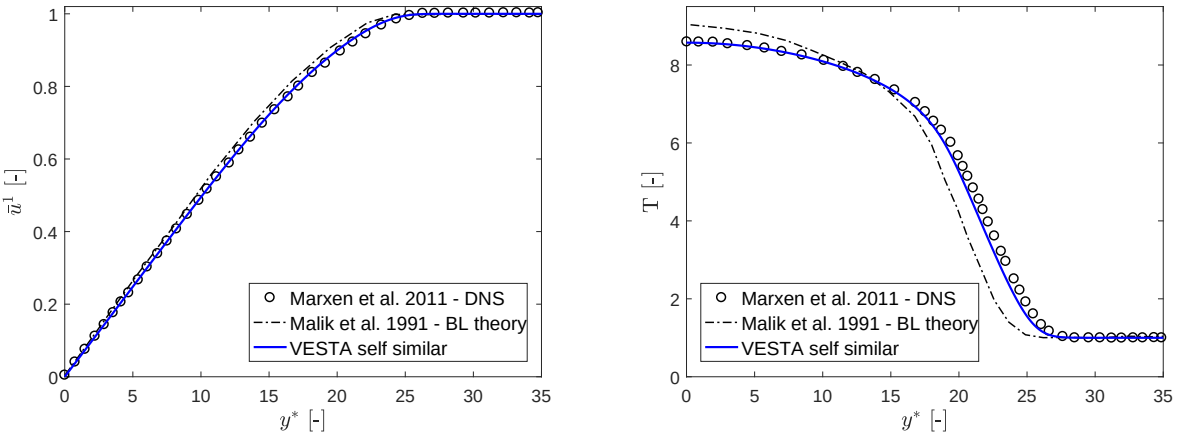

Figure 4: Streamwise velocity and temperature nondimensional mean flow profiles for the adiabatic Mach 10 flat plate case (see Tab. 2): comparison against Marxen et al.[19] and Malik et al.[16].

Despite the fact that this problem represents a benchmark case in hypersonic stability, at the author's knowledge, there are no examples of related PSE computations in literature. Chang et al.[4] reproduced the growth rate as a function of frequency at Re = 2000 with their PSE solver applied in the parallel flow limit, but they did not study eventual

DOI: 10.13009/EUCASS2017-288

Table 2: Studied test cases in hypersonic regime

M_e	T_e $[K]$	p_e $[Pa]$	Wall B.C.	F	Ref.
8	350	3596	$\partial T_w/\partial y = 0$	$3.40 \cdot 10^{-5}$	-
10	350	3596	$\partial T_w/\partial y = 0$	$3.40 \cdot 10^{-5}$	Malik et al.[16]/ Marxen et al.[19]
10	350	3596	$T_w/T_e = 3.43$	$3.40 \cdot 10^{-5}$	-
12	350	3596	$\partial T_w/\partial y = 0$	$3.40 \cdot 10^{-5}$	-

nonparallel effects. Fig. 5 displays the evolution of the streamwise velocity disturbance growth rate for a fix reduced frequency $F = 3.40 \cdot 10^{-5}$, computed by means of LST and PSE, in both CPG and LTE conditions. The reference solution of Malik et al.[16] is also marked. Even if the application of the high temperature gas model in the stability computations does not remarkably affect the growth rate peak maximum value, it leads to an evident shift of the curves towards lower Reynolds numbers. Most importantly, it gives inconsistent conclusions regarding the influence of nonparallel effects. In the CPG limit nonlocal effects tend to stabilize the flow with an upstream shift of the growth rate peak, while in LTE conditions there is a slight destabilization of the flow with a downstream movement of the maximum peak.

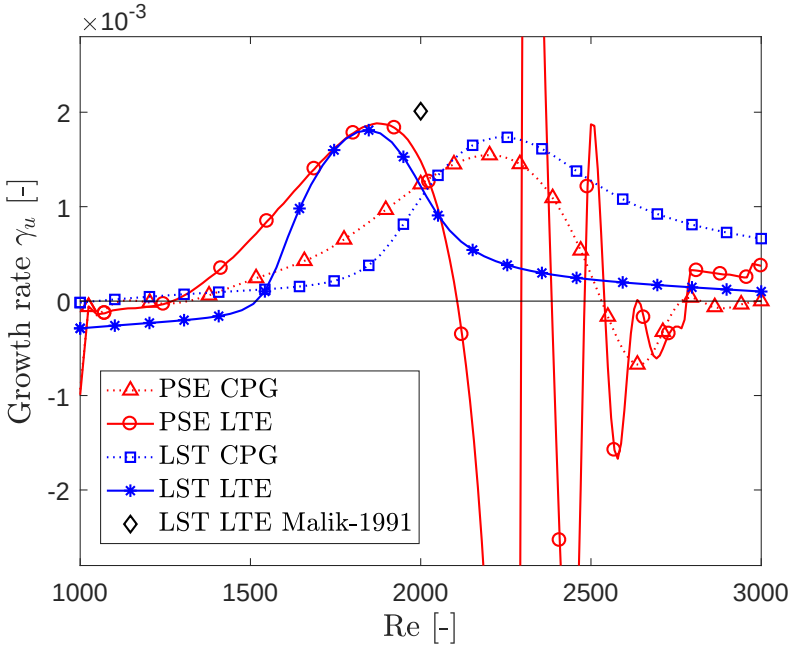

Figure 5: Growth rate in both CPG and LTE conditions: comparison against LST results and Malik et al.[16]. Adiabatic flow case: $M_e = 10$, $T_e = 350\,K$, $F = 3.40 \cdot 10^{-5}$

The PSE analysis captures oscillations in the growth rate that are not present in the LST counterpart, which decays more slowly, extending the instability region further downstream. They are stronger in the LTE case, even if additional simulations showed that an increment in the marching step can produce a moderate amplitude damping. This behavior was already reported by Chang et al.[4], for a different test case, and it was attributed to the presence of supersonic modes. Supersonic modes are characterized by a phase speed $c_r < 1 - 1/Ma_e$, and contrary to the subsonic ones they do not exponentially decay towards the freestream, but they manifest an oscillatory behavior also outside the boundary layer. Nevertheless, they are not acoustic waves since the amplitude of these oscillations is subjected to attenuation. Malik et al.[17] state that within LST, unstable supersonic modes generally appear when Dirichlet boundary conditions are applied. However, for this particular problem they claimed that extending the boundary layer edge imposing vanishing perturbations and applying the more correct asymptotic boundary conditions led to identical stability results[16]. Asymptotic and non-reflecting boundary conditions were also adopted within the PSE approach by Chang et al.[4]. On the other hand, supersonic mode capturing seems to be a feature of the PSE analysis itself. In particular, stronger consequences on the growth rate were reported with the chemical equilibrium model.

In order to exclude eventual modes synchronization from the possible causes of the solution oscillatory behavior

DOI: 10.13009/EUCASS2017-288

(see Fedorov et al.[7,6]), the phase speed diagram of the main discrete modes involved in the interested spatial domain were analyzed by means of a frequency sweeping within the LST in LTE conditions. The coexistence of multiple modes with identical shapes and phase speeds was speculated to cause the PSE algorithm to loose track of the Mack modes evolution. This coexistence is precisely what occurs at a synchronization point. Fig. 6 shows that the synchronization of modes S and F (according to the nomenclature in Fedorov[5]) occurs before the oscillations start, with no other modes found that could lead to further synchronizations.

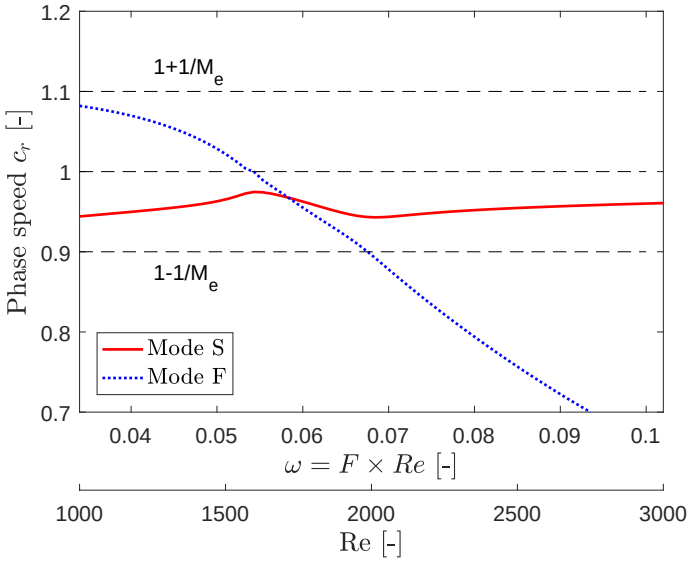

Figure 6: Phase speed diagram computed by LST. Adiabatic flow case: $M_e = 10$, $T_e = 350\,K$, $Re = 2000$

The PSE solver seems to correctly track the same mode identified by the LST. Fig. 7 displays a comparison of the amplitude functions of the streamwise velocity and pressure perturbations, normalized by the maximum amplitude of the streamwise velocity, computed by means of PSE and LST, at different Reynolds numbers. Despite some amplitude differences, accentuated in particular inside the oscillatory region, both analysis retrieve the same perturbations shapes. On the other hand, disturbances computed by PSE do not decay towards the freestream in the same way as the LST ones, but they show oscillations that persist also outside of the boundary layer (the boundary layer height is about $y_e/l_e = 26$). This confirms the observations made by Chang et al.[2].

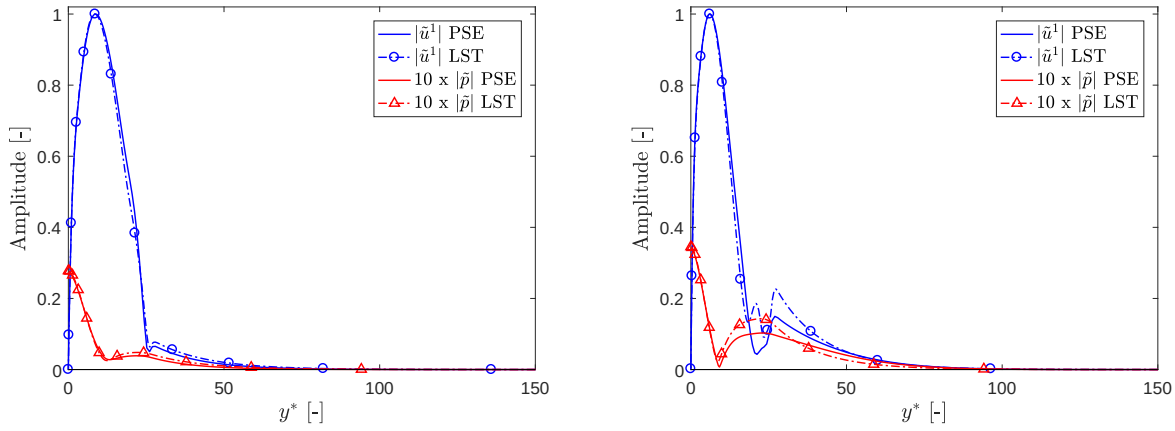

(a) Re=1800 (b) Re=2200

DOI: 10.13009/EUCASS2017-288

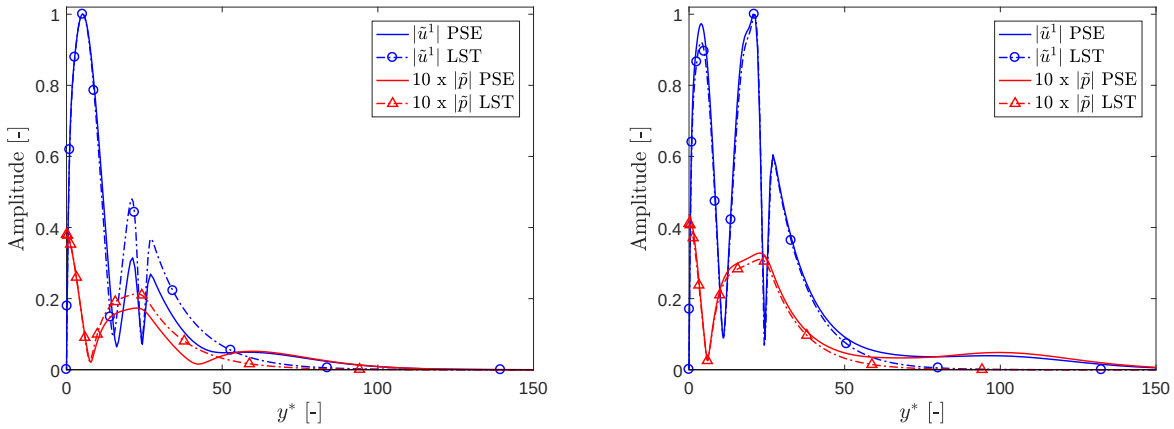

(c) Re=2400 (d) Re=2800

Figure 7: Amplitude functions of the streamwise velocity and pressure perturbations at different Reynolds numbers: comparison between the PSE and LST results in LTE conditions. Adiabatic flow case $M_e = 10$, $T_e = 350\,K$, $F = 3.40 \cdot 10^{-5}$

Moreover, plotting the streamwise velocity disturbance phase speed (Fig. 8) highlights a region around Re=2150 where the mode is supposed to be supersonic. The behavior of the curve further downstream, although already seen for example in Fig.8 in Marxen et al.[18], is not yet explained and needs additional investigations. Also, the pressure perturbation contour plot (real part), not shown here, puts in evidence a wave structure appearing on the downstream zone of the domain. This was identified in Chang et al.[2] (see Fig.17 of the cited reference) as a intermediate region in the mode switching from subsonic to supersonic.

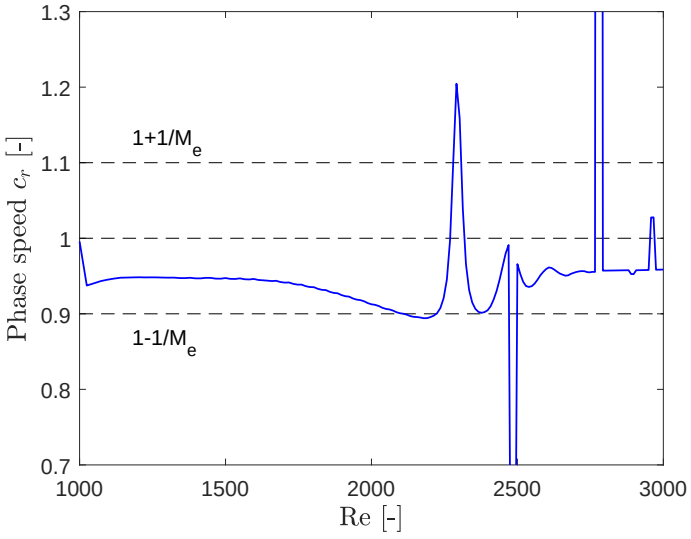

Figure 8: Phase speed of the streamwise velocity disturbance. Adiabatic flow case: $M_e = 10$, $T_e = 350\,K$, $F = 3.40 \cdot 10^{-5}$

Further studies are required in order to better understand and investigate the phenomena leading to the appearance of eventual unstable supersonic modes. To this end, the development of more consistent freestream boundary conditions (whether asymptotic or non-reflecting) will be pursued. Even if the boundary layer domain has been extended in the wall normal direction, and even if no perturbation oscillations were found to reach the upper computation domain boundary, the consequences of applying one type of boundary condition rather than another are still not clear.

An additional verification of the VESTA PSE algorithm is carried out by comparing in Fig. 9 the amplitude functions of the second Mack mode disturbance at Re=2000. All quantities are normalized with the maximum amplitude

DOI: 10.13009/EUCASS2017-288

of the streamwise velocity. The results obtained fit quite accurately the DNS ones and display some discrepancies compared to the LST curves, especially regarding the temperature perturbation. This is caused by the differences in the mean flow (Fig.4), since the regions of stronger variations coincide both for velocity and temperature. It is worth highlighting that the disagreement between the DNS and LST pressure curves close to the wall is just caused by a different nondimensionalization of the quantity. By making the pressure perturbation nondimensional with the mean boundary layer pressure value, as done in Malik et al.[16], the PSE result better matches the LST one. It is therefore reasonable to think that the DNS pressure disturbance would also behave in the same way. This was not pointed out in Marxen et al.[19].

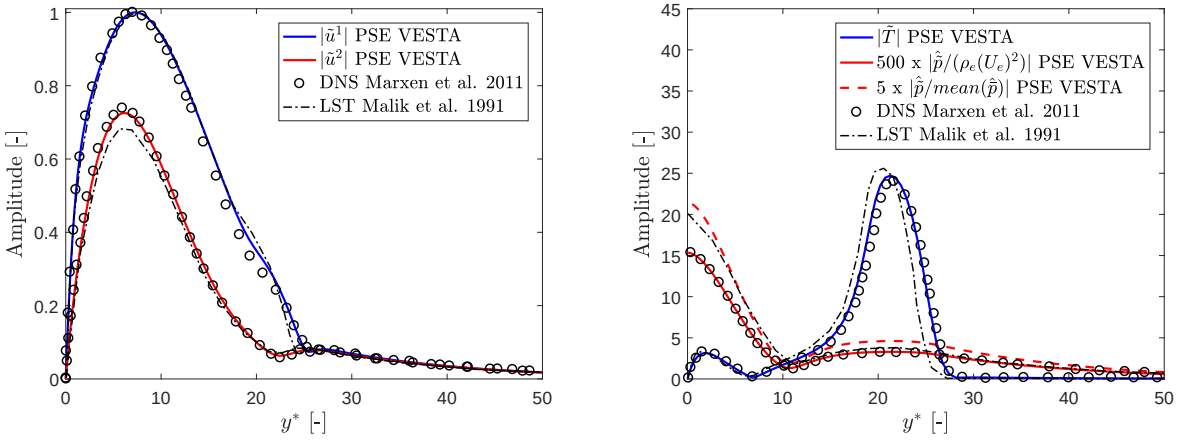

Figure 9: Amplitude functions of the second Mack mode: comparison against Marxen et al.[19] and Malik et al.[16]. Adiabatic flow case $M_e = 10$, $T_e = 350\,K$, $F = 3.40 \cdot 10^{-5}$, $Re = 2000$

Apart from differences which can be easily explained mainly with discrepancies in the mean flow models, the PSE code can be considered verified against the presented literature results for CPG and LTE conditions. In the following a study is carried out on how high temperature and nonlocal effects are affected by variations in the Mach and wall boundary condition. The following PSE simulations exhibit the same oscillatory phenomenon in the growth rate described in Fig.5, as well as the same features in the disturbance phase speed and pressure field plots. To have a better visualization of the results, the oscillations, which always occur at the end of the growth rate curve, were removed in Fig.11 - Fig.12.

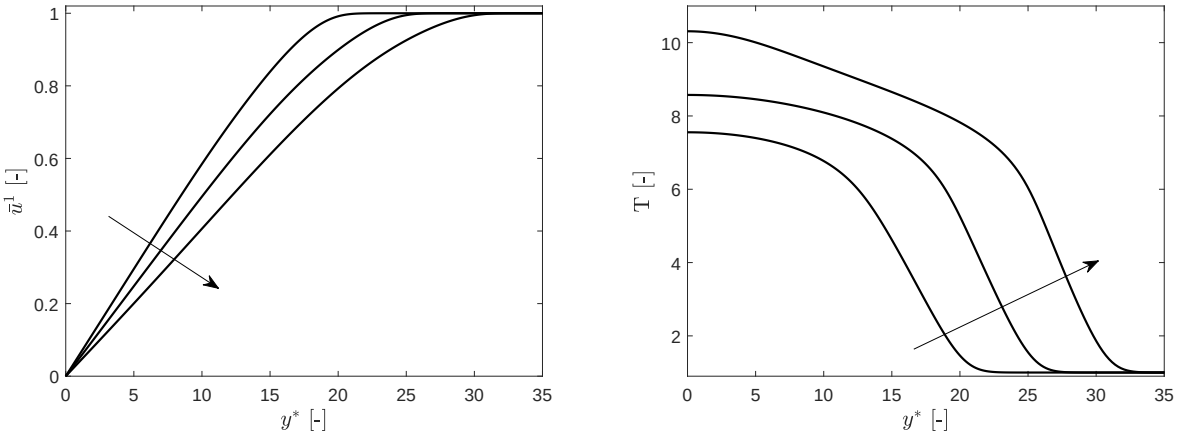

Figure 10: Streamwise velocity and temperature nondimensional mean flow profiles at Mach number 8,10, and 12, for freestream conditions of Tab. 2 and adiabatic wall. The arrow indicates increasing Mach

DOI: 10.13009/EUCASS2017-288

The effect of varying the Mach number is investigated by considering two additional flows at Mach 8 and 12, with the other same freestream conditions of the previously studied Mach 10 flow (see Tab. 2). The streamwise velocity and temperature profiles of the mean flows are collected in Fig.10. Increasing Mach leads to a hotter boundary layer. As a consequence, there is a stabilization of the second Mack mode as Fig.11 shows. The LTE results in Fig.11(a) reveal that nonparallel effects tend to become more significant as the Mach is increased, leading to a more unstable behavior. The same trend is observed in the CPG analysis (Fig.11(b)). However, in this case nonlocal effects gain importance more slowly with increased Mach, resulting that at Mach 12 LST still predicts a more unstable disturbance than PSE. This explains the inconsistency observed in Fig.5 when interpreting the nonparallel effects. It has to be noticed that in LTE, PSE shifts the growth rate towards higher Re than LST, while the shift appears in the opposite direction in the CPG solution. Accounting for high temperature effects also within the same stability theory is fundamental as Fig.11(c) displays. The LTE model predicts a more unstable boundary layer with an early appearance of a narrower instability region.

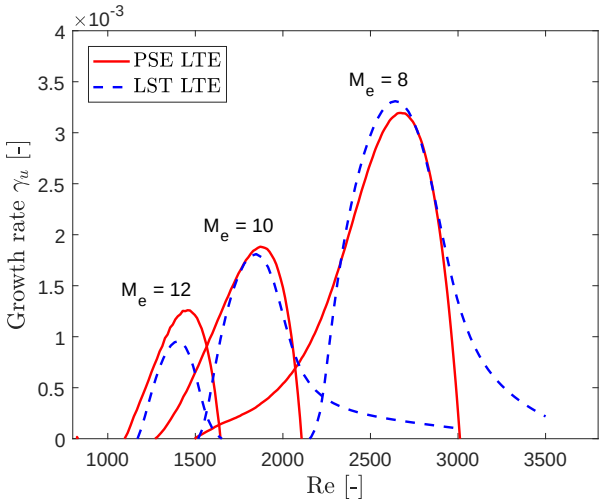

(a) PSE LTE vs. LST LTE

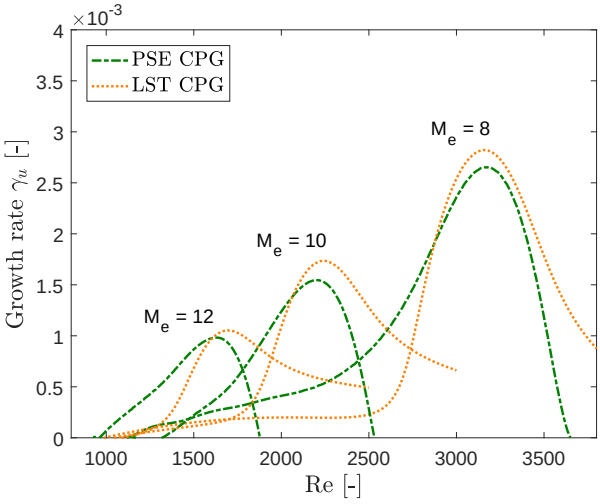

(b) PSE CPG vs. LST CPG

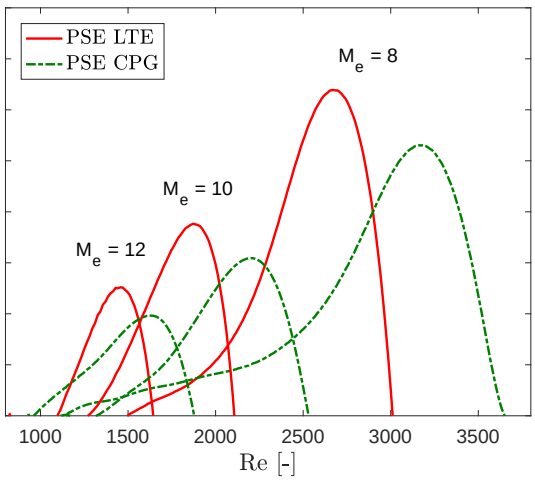

(c) PSE LTE vs. PSE CPG

Figure 11: Growth rate at different Mach numbers. Adiabatic flow case: $T_e = 350\,K$, $F = 3.40 \cdot 10^{-5}$

DOI: 10.13009/EUCASS2017-288

Finally, the effect of wall cooling is considered by taking the Mach 10 flow and imposing a wall temperature $T_w = 1200\,K$. The temperature mean flow becomes colder and almost no chemical activity occurs. Fig.12(a) shows the growth rate curves, computed by means of both parallel and nonparallel analysis in LTE conditions, for an adiabatic and an isothermal wall. As expected the cooling effect destabilizes the 2D second Mack mode and shifts the curves towards higher Re numbers: in this sense the PSE and LST solutions behave in the same way. In LTE nonlocal effects have the same influence found in the adiabatic case at the corresponding Mach. Nevertheless, Fig.12(b) shows the behavior in CPG conditions is different whether an adiabatic or isothermal wall is considered. While the former predicts a stabilization due to nonlocal effects, the latter shows a destabilization. Hence, most probably nonparall effects do not vary with the Mach number in the same way depending on the wall boundary condition. The importance of correctly taking into account high temperature effects is again evident when the LTE PSE results with the corresponding counterparts in CPG conditions are compared. Fig.12(c) shows that also with an isothermal wall the LTE model leads to a shift of the growth rate maximum towards lower Re. However, compared to the adiabatic wall, it produces a weaker destabilization of the flow.

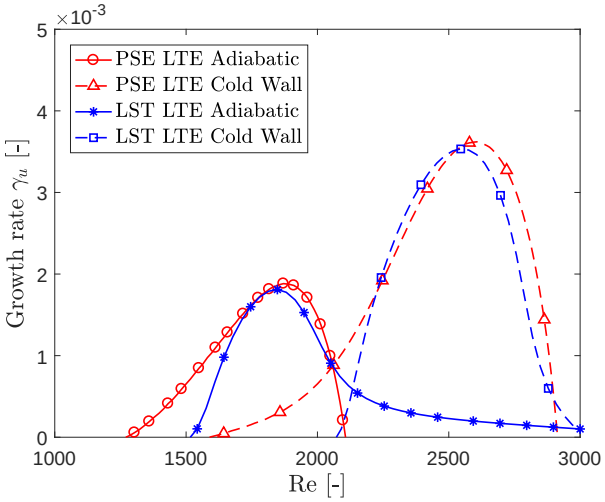

(a) PSE LTE vs. LST LTE

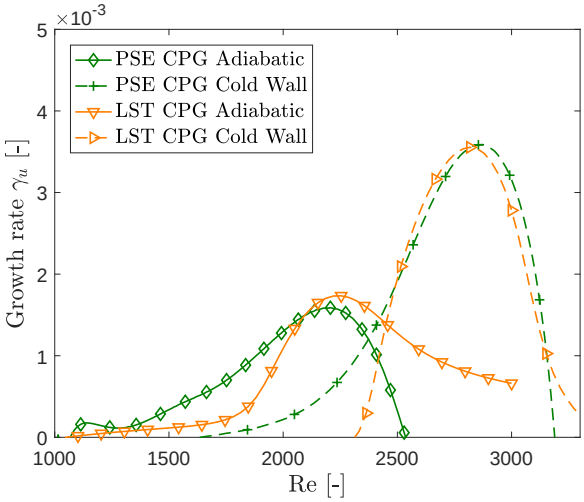

(b) PSE CPG vs. LST CPG

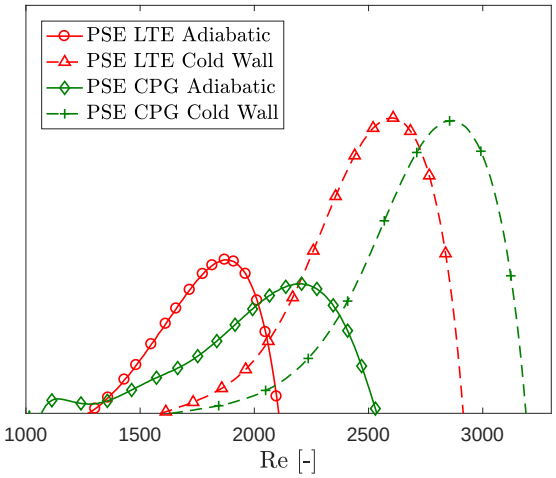

(c) PSE CPG vs. PSE LTE

Figure 12: Growth rate: comparison between adiabatic and isothermal wall boundary condition. Flow case: $M_e = 10$, $T_e = 350\,K$, $F = 3.40 \cdot 10^{-5}$

DOI: 10.13009/EUCASS2017-288

4. Conclusions

Stability of 2D disturbances in hypersonic flows over adiabatic and isothermal flat plates were studied by means of linear PSE, both for calorically perfect gas and local thermodynamic equilibrium conditions. The code was successfully verified against the literature. Some discrepancies were found in the high Mach test cases, but they can be related to differences in the mean flow computations due to the utilization of different aerothermodynamic models.

Accounting for high temperature effects revealed to be very important for the flow stability analysis. Not only it changes the growth rate curves within the same stability theory, but it can also lead to different quantitative and qualitative conclusions regarding the influence of nonparallel effects. Generally, considering the flow in LTE conditions rather than in CPG highlights a tendency to stabilize the first Mack mode at subsonic and low supersonic Mach numbers and to destabilize the second Mack mode in high supersonic and hypersonic regimes. In this regard it acts on the boundary layer stability like a cooling effect, since chemical activity usually cools down the temperature mean flow. It also produces a shift of the growth rate curve, but its direction depends once again on the regime. It was towards higher Reynolds numbers for the subsonic and supersonic cases, and towards lower Re for hypersonic cases.

Nonlocal effects have an influence on stability which depends on the Mach number. It was found, for the second Mack mode, that nonparallelism can switch from being stabilizing to destabilizing as the Mach increases. The destabilizing effect becomes stronger with increased Mach. The same trend can be observed also in the CPG limit, but the impact seems to be much smaller. The result is that at a specific Mach, discordant conclusions can be drawn about nonlocal effects, depending on the flow assumption considered. Moreover, the PSE analysis predicts a smaller instability region compared to the LST one, slightly moving it towards higher Re in LTE and towards lower Re in CPG.

The known destabilizing effect of wall cooling on the second Mack mode due to an isothermal wall boundary condition is not affected by the flow assumption adopted. The same conclusion of the adiabatic case can be inferred, but the destabilizing effect of assuming LTE is weaker with an isothermal cold wall.

Oscillations in the growth rate right after the instability region were found in all the PSE test, especially in LTE, as already reported in literature. The likely cause of this phenomenon seems to be confirmed by a switching of the tracked mode from subsonic to supersonic. However, further investigation is needed for a better understanding.

5. Acknowledgments

This research is made possible thanks to the financial support provided by the Fonds de la Recherche Scientifique through their FRIA fellowship program.

References

[1] F. P. Bertolotti. *Linear and nonlinear stability of boundary layers with streamwise varying properties*. PhD Thesis, The Ohio State University, 1991.

[2] C. L. Chang, M. Malik, G. Erlebacher, and M. Hussaini. Compressible stability of growing boundary layers using parabolized stability equations. *AIAA Paper 91-1636*, 1991.

[3] C.-L. Chang, M. R. Malik, G. Erlebacher, and M. Y. Hussaini. Linear and nonlinear PSE for compressible boundary layers. ICASE Report N. 93-70, NASA, 1993.

[4] C.-L. Chang, H. Vinh, and M. R. Malik. Hypersonic boundary-layer stability with chemical reactions using pse. In AIAA, editor, *28th Fluid Dynamic Conference*, 1997.

[5] A. V. Fedorov. High-speed boundary layer instability: old terminology and a new framework. *AIAA Journal*, 49(8), August 2011.

[6] A. V. Fedorov. Transition and stability of high-speed boundary layer. *Annual Review of Fluid Mechanics*, 43:79–95, 2011.

[7] A. V. Fedorov and A. P. Khokhlov. Prehistory of instability in hypersonic boundary layer. *Theoretical and Computational Fluid Dynamics*, 14:359–375, 6, 2001.

[8] K. Groot. *Error free derivation of Parabolized Stability Equations*. Short Training Report, Von Karman Institute, 2013-06.

[9] T. Herbert. Parabolized stability equations. In AGARD, editor, *Special Course on Progress in Transition Modeling*, number R-793, 1993.

[10] T. Herbert and F. P. Bertolotti. Stability analysis of nonparallel boundary layers. *Bulletin of the American Physical Society*, 32:2079, 1987.

DOI: 10.13009/EUCASS2017-288

[11] M. L. Hudson, N Chokani, and G. V. Candler. Linear stability of hypersonic flow in thermochemical nonequilibrium. *AIAA J.*, 35(6), 1996.

[12] H. B. Johnson and G. V. Candler. Hypersonic boundary layer stability analysis using pse-chem. In AIAA, editor, *35th AIAA Fluid Dynamics Conference*, Toronto, Ontario, Canada, 2005.

[13] H. B. Johnson and G. V. Candler. Pse analysis of reacting hypersonic boundary layer transition. In AIAA, editor, *30th AIAA Fluid Dynamics Conference*, Norfolk, VA, 1999.

[14] T. E. Magin and G. Degrez. Transport algorithms for partially ionized and unmagnetized plasmas. *Journal of Computational Physics*, 198:424–449, 2, 2004.

[15] M. R. Malik. Hypersonic flight transition data analysis using parabolized stability equations with chemistry effects. *Journal of Spacecraft and Rockets*, 40(3), 2003.

[16] M. R. Malik and E. C. Anderson. Real gas effects on hypersonic boundary-layer stability. *Physics of Fluids A*, 3(5):803–820, 1991.

[17] M. R. Malik and R. E. Spall. On the stability of compressible flow past axisymmetric bodies. *Journal of Fluid Mechanics*, 228:443–463, 1991.

[18] G. Marxen O. Iaccarino and T. Magin. Direct numerical simulations of hypersonic boundary-layer transition with finite-rate chemistry. *Journal of Fluid Mechanics*, 755:35–49, 2014.

[19] O. Marxen, T. Magin, G. Iaccarino, and S. G. Shaqfeh. A high-order numerical method to study hypersonic boundary layer instability including high-temperature gas effects. *Physics of Fluids*, 23, 2011.

[20] F. Pinna. *Numerical study of stability of flows from low to high Mach number*. PhD thesis, Von Karman Institute - Università degli Studi di Roma La Sapienza, 2012.

[21] F. Pinna and K. Groot. Automatic derivation of stability equations in arbitrary coordinates and different flow regimes. In AIAA, editor, *44th Fluid Dynamic Conference*, 2014.

[22] H. L. Reed, R. Kimmel, S. Scheider, and D. Arnal. Drag prediction and transition in hypersonic flow. *AIAA Paper 97-1818*, 1997.

[23] H. L. Reed, E. Perez, J. Kuehl, T. Kocian, and N. Oliviero. Verification and validation issues in hypersonic stability and transition prediction. *Journal of Spacecraft and Rockets*, 52(1):29–37, 2014.

[24] H. Salinas. *Stabilité linéaire et faiblement non linéaire d'une couche limite laminaire compressible tridimensionnelle par l'approche PSE*. PhD thesis, École National Supérieure de l'Aéronautique et de l'Espace, 1998.

[25] J. B. Scoggins and T. E. Magin. Development of mutation++: multicomponent thermodynamic and transport properties for ionized plasmas written in c++. In AIAA, editor, *11th AIAA/ASME Joint Thermophysics and Heat Transfer Conference*, number AIAA 2014-2966, 2014.

[26] J. B. Scoggins and T. E. Magin. Gibbs function continuation for linearly constrained multiphase equilibria. *Combustion and Flame*, 162, 2015.

[27] G. Stuckert and H. L. Reed. Linear disturbances in hypersonic chemically reacting shock layers. *AIAA J.*, 32(7), 1994.

[28] L. Zanus. Analysis of a compressible boundary layer flow by means of parabolized stability calculations. Research Master report 2016-28, von Karman Institute, June, 2016.